Mon. Not. R. Astron. Soc. **000**, 000–000 (0000) Printed 20 December 2011 (MN LaTeX style file v2.2)

Internal shock model for the X-ray flares of Swift J1644+57

F. Y. Wang[1,2,3] and K. S. Cheng[1]
[1] Department of Physics, The University of Hong Kong, Pokfulam Road, Hong Kong, China
[2] Department of Astronomy, Nanjing University, Nanjing 210093, China
[3] Key Laboratory of Modern Astronomy and Astrophysics (Nanjing University), Ministry of Education, Nanjing 210093, China

20 December 2011

ABSTRACT
Swift J1644+57 is an unusual transient event, likely powered by the tidal disruption of a star by a massive black hole. There are multiple short timescales X-ray flares were seen over a span of several days. We propose that these flares could be produced by internal shocks. In the internal shock model, the forward and reverse shocks are produced by collisions between relativistic shells ejected from central engine. The synchrotron emission from the forward and reverse shocks could dominate at two quite different energy bands under some conditions, the relativistic reverse shock dominates the X-ray emission and the Newtonian forward shock dominates the infrared and optical emission. We show that the spectral energy distribution of Swift J1644+57 could be explained by internal shock model.

Key words: radiation mechanisms: non-thermal - X-rays: general

1 INTRODUCTION

Swift J1644+57 was triggered by the Swift/BAT on 28 March 2011 (Cummings et al. 2011). Swift J1644+57 was initially discovered as a long-duration gamma-ray burst (GRB 110328A) by the Swift satellite, but the light curve soon showed that it was quite different. It remained bright and highly variable for a long period, and re-trigger the BAT three times over the next 48 hours (Sakamoto et al. 2011). The isotropic X-ray luminosity of Swift J1644+57 ranges from $10^{45} - 4 \times 10^{48}$ erg s^{-1}, and the total isotropic energy is about 3×10^{53} erg during the first 30 days after the BAT trigger (Burrows et al. 2011). From the strong emission lines of hydrogen and oxygen, Levan et al. (2011) estimate the redshift of Swift J1644+57 is $z = 0.35$. From the astrometric observation of the X-ray, optical, infrared, and radio transient with the light-centroid of the host galaxy, it is found that the position of this source is consistent with arising in the nucleus of the host galaxy (Bloom et al. 2011; Zauderer et al. 2011).

The X-ray light curve of Swift J1644+57 exhibits repeated extremely short timescale flares. The flares have rise-times as short as 100 s (Burrows et al. 2011). These flares are similar as the flares discovered in the GRB afterglow (Burrows et al. 2005), which may indicate the same origin of them. The internal shock model can produce the X-ray flares observed in GRB afterglows (Burrows et al. 2005; Fan & Wei 2005; Zhang et al. 2006; Yu & Dai 2009).

After the Swift J1644+57 was discovered, several models were proposed to explain it, most concentrating on a picture that a main sequence star was tidally disrupted by passing too close to a $10^6 - 10^7 M_\odot$ black hole (Bloom et al. 2011; Burrows et al. 2011; Cannizzo et al. 2011; Socrates 2011; Shao et al. 2011). Krolik & Piran (2011) suggest that this event may be produced by a white dwarf tidally disrupted by a $10^4 M_\odot$ black hole. The process is as follow: a star is disrupted as it passes near a supermassive black hole, and much of its mass is distributed into an accretion disk around the black hole. A powerful jet is then launched. In these models, the X-ray emission is thought to be produced by external inverse Compton (EIC) (Bloom et al. 2011) or synchrotron emission (Burrows et al. 2011). But on the high frequency side, the Fermi LAT (Campana et al. 2011) and VERITAS upper limits (Aliu et al. 2011) require that the synchrotron self-Compton (SSC) component is suppressed by $\gamma - \gamma$ pair production. The soft photons of $\gamma - \gamma$ pair production are thought to be generated from the thermal emission of the accretion disk or the disk outflow. In the SSC model, soft photons originated from the thermal emission of the accretion disk may not provide an efficient source for the $\gamma - \gamma$ production. Because the condition of $\gamma - \gamma$ production is $E_X E_\gamma (1 - \cos\theta) \geqslant 2(m_e c^2)^2$, where θ is the angle between the directions of soft seed photon and high-energy photon. Only a fraction of high-energy emission can be absorbed by soft photons. So the soft photons from the disk outflow may be a better candidate (Strubbe & Quataert 2009). In the synchrotron emission model, the jet must have a strong magnetic field (Poynting-flux-dominated) and has

ongoing in situ acceleration of electrons (Aliu et al. 2011; Burrows et al. 2011).

In this letter, we use the internal shock model to explain the X-ray flares of Swift J1644+57. The internal shock produces the prompt emission of GRB in the standard fireball model (Rees & Mészáros 1994; Paczyński & Xu 1994). The internal shock model also the leading model of X-ray flares in GRBs, the external shock model is very hard to account for the X-ray flares (Burrows et al. 2005; Fan & Wei 2005). The central engine of this event may be formed as follow. When a supermassive black hole tidal disrupts a star, a disk is formed. The magnetic field could be produced by disk instability. The disk can then anchor and amplify the seed magnetic field to a strong ordered poloidal field , which in turn threads the black hole with debris material in the inner region of the disk. A large amount of the rotational energy of the black hole can be extracted via the Blandford-Znajek (BZ) process, which creates a jet along the rotation axis (Blandford & Znajek 1977). The magnetic field lines will break the disk into blobs, so many shells could be ejected (Cheng & Lu 2001). When fast shell catches up with early slow shell, internal shock is generated. Other models of central engine also discussed, such as the episodic accretion onto a central object due to a chopped accretion disk (Perna et al. 2006), or episodic accretion due to a modulation of the accretion flow by a magnetic barrier (Proga & Zhang 2006).

The structure of this letter is as follow. In next section, we describe the dynamics of internal shock arising from a collision between two shells and the synchrotron radiation of the shocked electrons. In Section 3, we apply the model to the Swift J1644+57. Finally, a summary is given in Section 4.

2 THE INTERNAL SHOCK MODEL

The internal shock model has been extensively discussed in literature (Rees & Mészáros 1994; Paczynski & Xu 1994; Yu & Dai 2009; Yu, Wang & Dai 2009). We give a brief description of our model as follow. Shells with different Lorentz factors and densities are ejected by the central black hole. Collisions of a pair of ejecta can produce different intensities of X-rays. For example two shells with similar Lorentz factor and density will produce a weak flare whereas two shells with large differences can produce a strong flare. Since the collision frequency of these pairs (internal shocks) should be very high, it should result in rapid variable intensities. Simultaneously some earlier ejected fast moving shells can already reach the interstellar medium(ISM) and produce the external shock there (Sari & Piran 1995). Since the earlier ejected shells are less and hence the radiation results from external shock should be weak in the beginning. However after collisions of pairs they can merge and move toward the ISM and provide more energy into the external shock. Therefore the radiation intensity due to the external shock should gradually increase. We should note that since the injected energy provided in this way is in a discrete manner, therefore the flux will increase substantially but gradually decrease back to the original light curve. This phenomenon is similar to that observed in GRBs known as "re-brightening" effect (Zhang & Mészáros 2002; Huang et al. 2006). In Figure 1 we provide a schematic illustration of our model.

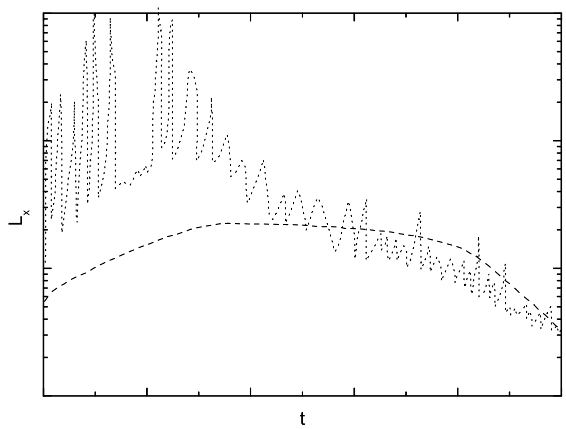

Figure 1. Schematic illustration of the model. The dotted line represents the intensity produced by internal shocks. The dashed line represents the intensity produced by the external shock. In this figure we argue that large short-term fluctuations can still occur due to collisions of few later ejecta when the jet still exists.

2.1 Shock dynamics

At a time of t_A, the central engine ejects a shell denoted by A with bulk Lorentz factor $\gamma_{\rm A}$ with isotropic kinetic energy luminosity $L_{\rm A}$. Some time (δt) later, another shell B with $\gamma_{\rm B}$ and $L_{\rm B}$ is assumed to be ejected. In order to let shell B catch up and collide with the shell A, $\gamma_{\rm B} > \gamma_{\rm A}$ is required. At the radius $R_{\rm col} = \beta_{\rm A}\beta_{\rm B}c\delta t/\psi(z)(\beta_{\rm B}-\beta_{\rm A})$, a collision between A and B takes place. For $(\gamma_{\rm A},\gamma_{\rm B}) \gg 1$, The collision radius is (Yu & Dai 2009)

$$R_{\rm col} \simeq \frac{2\gamma_{\rm A}^2 c\delta t}{(1-(\gamma_{\rm A}/\gamma_{\rm B})^2)\psi(z)}, \tag{1}$$

where $\psi(z) = 1+z$.

After the collision, a forward shock and a reverse shock are produced. The system is separated into four regions by the two shocks and a contact discontinuity surface: (1) unshocked shell A, (2) shocked shell A, (3) shocked shell B, and (4) unshocked shell B, bulk Lorentz factors of which are $\gamma_1 = \gamma_{\rm A}$, $\gamma_2 = \gamma_3 \equiv \gamma$, and $\gamma_4 = \gamma_{\rm B}$. Two relative Lorentz factors of the shocked regions relative to unshocked regions 1 and 4, can be calculated by

$$\gamma_{21} = \frac{1}{2}\left(\frac{\gamma_1}{\gamma}+\frac{\gamma}{\gamma_1}\right), \quad \gamma_{34} = \frac{1}{2}\left(\frac{\gamma}{\gamma_4}+\frac{\gamma_4}{\gamma}\right). \tag{2}$$

According to Blandford & McKee (1976), the internal energy densities of the two shocked regions are $e_2 = (\gamma_{21}-1)(4\gamma_{21}+3)n_1 m_p c^2$ and $e_3 = (\gamma_{34}-1)(4\gamma_{34}+3)n_4 m_p c^2$, where $n_1 = L_{\rm A}/4\pi R_{\rm col}^2\gamma_{\rm A}^2 m_p c^3$ and $n_4 = L_{\rm B}/4\pi R_{\rm col}^2\gamma_{\rm B}^2 m_p c^3$. The mechanical equilibrium between the two shocked regions requires $e_2 = e_3$, so

$$\frac{(\gamma_{21}-1)(4\gamma_{21}+3)}{(\gamma_{34}-1)(4\gamma_{34}+3)} = \frac{n_4}{n_1} = \left(\frac{L_4}{L_1}\right)\left(\frac{\gamma_1}{\gamma_4}\right)^2 \equiv f, \tag{3}$$

where $L_1 = L_{\rm A}$ and $L_4 = L_{\rm B}$. We can calculate the values of γ, γ_{21} and γ_{34} from equations (2) and (3) after the param-

eters of shells are given. In four limit cases, these equations can be solved analytically (Yu & Dai 2009). For $\gamma_4 \gg \gamma_1$, (1) if $L_4/L_1 \gg (1/7)\,(\gamma_4/\gamma_1)^4$, we have $\gamma_{21} = \gamma_4/2\gamma_1 \gg 1$, $\gamma_{34} - 1 \approx \gamma_4^2/7f\gamma_1^2$ and $\gamma = \gamma_4(1 - \sqrt{2\xi})$, which means the forward shock is relativistic and the reverse shock is Newtonian; (2) if $16 \ll L_4/L_1 \ll (1/16)\,(\gamma_4/\gamma_1)^4$, we can obtain $\gamma_{21} = f^{1/4}\gamma_4^{1/2}/2\gamma_1^{1/2} \gg 1$, $\gamma_{34} = \gamma_4^{1/2}/2f^{1/4}\gamma_1^{1/2} \gg 1$ and $\gamma = f^{1/4}\gamma_1^{1/2}\gamma_4^{1/2}$, so both the two shocks are relativistic; (3) if $L_4/L_1 \ll 7$, we get $\gamma_{21} - 1 \approx f\gamma_4^2/7\gamma_1^2 = \xi$, $\gamma_{34} = \gamma_4/2\gamma_1$ and $\gamma = \gamma_1(1 + \sqrt{2\xi})$, so the forward shock is Newtonian and the reverse shock is relativistic. Finally, (4) for $\gamma_4 \approx \gamma_1$, both the two shocks are Newtonian. Since γ_1, γ_4, and f are unchanged with the moving of the shells, the values of γ ,γ_{21} and γ_{34} are constant before the shocks cross the shells (Yu & Dai 2009).

2.2 Synchrotron emission from forward and reverse shocks

Following Dai & Lu (2002), the total number of the electrons swept-up by the forward and reverse shocks during a period of δt can be expressed by $N_{e,2} = 2\sqrt{2\xi}L_A\delta t/\left(\psi(z)\gamma_1 m_p c^2\right)$ and $N_{e,3} = L_B\delta t/\left(\psi(z)\gamma_4 m_p c^2\right)$, respectively (Yu, Wang & Dai 2009).

The forward and reverse shocks can accelerate particles to high energies. Following Sari et al. (1998), we assume that the energies of the hot electrons and magnetic fields are fractions ϵ_e and ϵ_B of the total internal energy, respectively. Thus, the strength of the magnetic fields is $B_i = (8\pi\epsilon_{B,i}e_i)^{1/2}$, $\quad i = 2, 3$. We assume a power-law distribution of the shock-accelerated electrons, $dn_e/d\gamma_e \propto \gamma_e^{-p}$ for $\gamma_e \geqslant \gamma_{e,m}$ (Sari et al. 1998). The random Lorentz factor of electrons in regions 2 or 3 is determined by $\gamma_{e,m,i} = \epsilon_{e,i}\frac{m_p}{m_e}\frac{(p-2)}{(p-1)}(\Gamma - 1)$, where Γ equals to γ_{21} or γ_{34}. In both shocked regions, the hot electrons with energies above $\gamma_{e,c,i}m_e c^2$ lose most of their energies during a cooling time δt, where the cooling Lorentz factor is determined by $\gamma_{e,c,i} = 6\pi m_e c\psi(z)/\left(\sigma_T B_i^2\gamma\delta t\right)$. The two characteristic frequencies and a peak flux density are (Sari et al . 1998; Wijers & Galama 1999)

$$
\begin{aligned}
\nu_{m,i} &= \frac{q_e}{2\pi m_e c\psi(z)}B_i\gamma_{e,m,i}^2\gamma, \\
\nu_{c,i} &= \frac{q_e}{2\pi m_e c\psi(z)}B_i\gamma_{e,c,i}^2\gamma, \\
F_{\nu,\max,i} &= \frac{3\sqrt{3}\Phi(p)\psi(z)N_{e,i}m_e c^2\sigma_T B_i\gamma}{32\pi^2 q_e d_L^2},
\end{aligned}
\tag{4}
$$

where $d_L = c(1+z)/H_0\int_0^z \frac{dz'}{\sqrt{\Omega_M(1+z')^3+\Omega_\Lambda}}$ is the luminosity distance of the source and $\Phi(p)$ is a function of p, for $p = 2.2$, $\Phi(p) \approx 0.6$ (Wijers & Galama 1999). In the calculation, we use $\Omega_M = 0.3$, $\Omega_\Lambda = 0.7$ and H_0=70 km s^{-1} Mpc^{-1}. q_e is the electron charge and σ_T is the Thomson cross section. The synchrotron spectrum can be written as (Sari et al. 1998)

$$
F_{\nu,i} = F_{\nu,\max,i}\times
\begin{cases}
\left(\frac{\nu}{\nu_l}\right)^{1/3}, & \nu < \nu_l; \\
\left(\frac{\nu}{\nu_l}\right)^{-(q-1)/2}, & \nu_l < \nu < \nu_h; \\
\left(\frac{\nu_h}{\nu_l}\right)^{-(q-1)/2}\left(\frac{\nu}{\nu_h}\right)^{-p/2}, & \nu_h < \nu,
\end{cases}
\tag{5}
$$

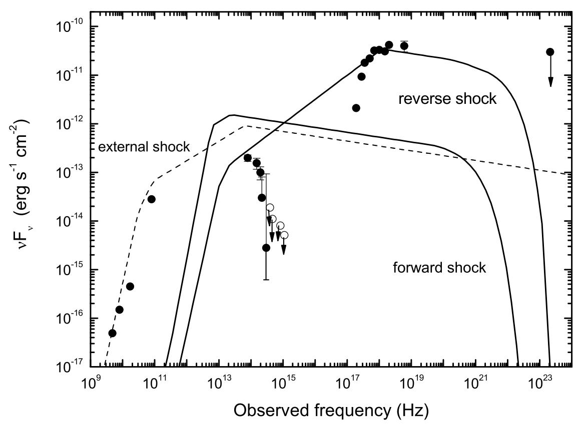

Figure 2. The broadband spectral energy distribution of Swift J1644+57 at 2.9 day after the BAT trigger. The points show the observation data, which are taken from Bloom et al. (2011). The two solid lines represent the unabsorbed spectrum of the reverse and forward shocks, which are generated by the internal shock. The dashed line shows the spectrum of external shock. In order to fit the spectrum, a moderate extinction ($A_V = 3-5$) is required.

where $\nu_l = \min(\nu_{m,i}, \nu_{c,i})$, $\nu_h = \max(\nu_{m,i}, \nu_{c,i})$, and $q = 2$ for $\nu_{c,i} < \nu_{m,i}$ and $q = p$ for $\nu_{c,i} > \nu_{m,i}$.

3 IMPLICATION FOR THE SWIFT J1644+57

There are two peaks in the spectrum of Swift J1644+57, far-infrared (FIR) and hard X-ray peaks. In order to fit the spectrum, we focus on the case (3) of internal shock model in section 2.1, in which the reverse shock is relativistic and the forward shock is Newtonian. In the rest of the paper we denote $Q = 10^x Q_x$. For illustration purpose, we set $L_4 = L_1 = L = 10^{47.0}$erg s^{-1}, $\gamma_4 = 1000$, $\gamma_1 = 10$, $\epsilon_{e,2} = \epsilon_{e,3} = \epsilon_e = 0.5$ and $\epsilon_{B,2} = \epsilon_{B,3} = \epsilon_B = 0.1$. **As shown in Cheng & Lu (2001), the Lorentz factor of shell can be up to** 1000**. It is reasonable to adopt** $\gamma_4 = 1000$**.** According to observation, we use $\delta t \sim 100$ s, the variability timescale of flare (Bloom et al. 2011; Burrows et al. 2011). The collision radius is $R_{\rm col} \sim 2\gamma_1^2 c\delta t/\psi(z) \sim 5\times10^{14}$cm, which is consistent with the X-ray emission radius determined from observation (Bloom et al. 2011). The Lorentz factor of merged shell is $\gamma \sim 14$. Using equation (4), we can obtain the following expressions for the reverse shock

$$
\begin{aligned}
\nu_{m,3} &\simeq 1.2\times10^{18}\ \mathrm{Hz}\ \epsilon_{e,-0.3}^2\gamma_{4,3}^2L_{47}^{1/2}\epsilon_{B,-1}^{1/2}\delta t_2^{-1}\gamma_{1,1}^{-4}, \\
\nu_{c,3} &\simeq 2.2\times10^{13}\ \mathrm{Hz}\ L_{47}^{-3/2}\epsilon_{B,-1}^{-3/2}\delta t_2\gamma_{1,1}^8, \\
F_{\nu,\max,3} &\simeq 0.9\ \mathrm{mJy}\ L_{47}^{3/2}\epsilon_{B,-1}^{1/2}\gamma_{1,1}^{-2}\gamma_{4,3}^{-1}d_{L,27.7}^{-2}.
\end{aligned}
\tag{6}
$$

For the forward shock, we obtain

$$
\begin{aligned}
\nu_{m,2} &\simeq 3.5\times10^{11}\ \mathrm{Hz}\ \epsilon_{e,-0.3}^2L_{47}^{1/2}\epsilon_{B,-1}^{1/2}\delta t_2^{-1}\gamma_{1,1}^{-2}, \\
\nu_{c,2} &\simeq 2.2\times10^{13}\ \mathrm{Hz}\ L_{47}^{-3/2}\epsilon_{B,-1}^{-3/2}\delta t_2\gamma_{1,1}^8, \\
F_{\nu,\max,2} &\simeq 15\ \mathrm{mJy}\ L_{47}^{3/2}\epsilon_{B,-1}^{1/2}\gamma_{1,1}^{-3}d_{L,27.7}^{-2}.
\end{aligned}
\tag{7}
$$

Therefore, the resulting synchrotron photons emitted by the two shocks are expected to peak at two different energy bands and thus two distinct spectral components[1].The peak of reverse shock spectrum will be at hard X-ray, but peak of the forward shock will be at FIR. The synchrotron self-absorption must be taken into account. In $\nu_{m,2} < \nu_{a,2} < \nu_{c,2}$ case, the synchrotron self-absorption frequency in region 2 reads (Panaitescu & Kumar 2000)

$$\nu_{a,2} = \left(\frac{5q_e N_{e,2}}{4\pi R_{\rm col}^2 B_2 \gamma_{e,m,2}^5}\right)^{2/(p+4)} \nu_{m,2}$$
$$\simeq 6.0\times10^{12}\ {\rm Hz}\ \epsilon_{e,-0.3}^{\frac{2p-2}{p+4}} L_{47}^{\frac{6+p}{2(p+4)}} \epsilon_{B,-1}^{\frac{p+2}{2(p+4)}} \gamma_{1,1}^{-\frac{12+2p}{p+4}}. \quad (8)$$

In $\nu_{a,3} < \nu_{c,3} < \nu_{m,3}$ case, the synchrotron self-absorption frequency in region 3 can be calculated by (Panaitescu & Kumar 2000)

$$\nu_{a,3} = \left(\frac{5q_e N_{e,3}}{4\pi R_{\rm col}^2 B_3 \gamma_{e,c,3}^5}\right)^{3/5} \nu_{c,3}$$
$$\simeq 1.0\times10^{13}\ {\rm Hz}\ \epsilon_{B,-1}^{6/5} L_{47}^{8/5} \gamma_{4,3}^{-3/5} \gamma_{1,1}^{-38/5} \delta t_2^{-2}. \quad (9)$$

The maximum Lorentz factor is limited by the synchrotron losses and is given by (Cheng & Wei 1996)

$$\gamma_{M,i} \simeq (3q_e/B_i\sigma_T)^{1/2} \simeq 4\times10^7 B_i^{-1/2}. \quad (10)$$

Another mechanism to restrict the maximum energy of an electron is diffusion. It turns out that maximum Lorentz factor restricted by diffusion is much larger than that in equation (10). So The maximal synchrotron photon energy can be estimated (Fan & Piran 2008)

$$h\nu_{M,i} \simeq \frac{hq_e B_i}{2\pi m_e c\psi(z)} \gamma_{M,i}^2 \Gamma \sim \frac{30\Gamma}{1+z}\ \ {\rm MeV}, \quad (11)$$

where h is the Planck constant, Γ equals to γ_{21} or γ_{34}.

The spectrum of internal shock model is shown in Figure 2 using above parameters during a high state. The X-ray spectrum of Swift J1644+57 can be generated in our model. A moderate extinction ($A_V \sim 3-5$) is required to explain the spectrum. This value of extinction is reasonable in this case, because of this event is arising in the nucleus of host galaxy. This value is also consistent with that determined by Bloom et al. (2011) and Burrows et al. (2011). Because of large value of synchrotron self-absorption frequency, the radio emission of internal shock is suppressed. From observations, the radio emission is from larger radius comparing with X-ray emission (Bloom et al. 2011; Burrows et al. 2011). The interaction between the first shell ejected by central engine and the ISM results in an external shock. The radio emission is from large radius and can be modeled by this external shock, similar as GRB afterglow.

The total energy release during this initial period is about $E_{\rm iso} \sim 10^{53}$erg (Bloom et al. 2011). The ISM density is about $n \sim 10{\rm cm}^{-3}$. Following Sari et al. (1998) and Bloom et al. (2011), we obtain the synchrotron frequencies and peak flux of external shock as follow

$$\nu_a \simeq 2.0\times10^{10}\ {\rm Hz}\ \epsilon_{e,-1}^{-1}\epsilon_{B,-2}^{1/5}E_{53}^{1/5}n_1^{3/5},$$
$$\nu_m \simeq 3.0\times10^{11}\ {\rm Hz}\ \epsilon_{e,-1}^{2}\epsilon_{B,-2}^{1/2}E_{53}^{1/2}t_{\rm days}^{-3/2},$$
$$\nu_c \simeq 8.0\times10^{13}\ {\rm Hz}\ \epsilon_{B,-2}^{-3/2}E_{53}^{-1/2}n_1^{-1}t_{\rm days}^{-1/2},$$
$$F_{\nu,\max} \simeq 170\ {\rm mJy}\ \epsilon_{B,-2}^{1/2}E_{53}n_1^{1/2}t_{\rm days}^{-3/4}d_{L,27.7}^{-2}. \quad (12)$$

The expression of $F_{\nu,\max}$ is a little different from that of Sari et al. (1998), because the observer has already observed the edges of the jet, as discussed in Bloom et al. (2011). The spectrum of the external shock is shown as dashed line in figure 2, which can only produce a simple power law in X-ray region. The radio light curve is different from $t^{-5/3}$ behavior observed the late X-ray light curve (Giannios & Metzger 2011; Metzger et al. 2011) because the radio light curve should be determined by the evolution of the external shock and has nothing to do with the accretion rate in the disk.

So our model predicates that, during the high state (flaring), the emission of internal shock will dominate at X-ray band and a broken power-law spectrum is shown. During the low state (no flares), there is no internal shocks and the emission is from the external shock. Because the typical frequencies of external shock is low at the first few days (see equation (12)), the spectrum at X-ray band exhibits as a single power-law if no energy injection happens. In both states, the radio emission is from the external shock.

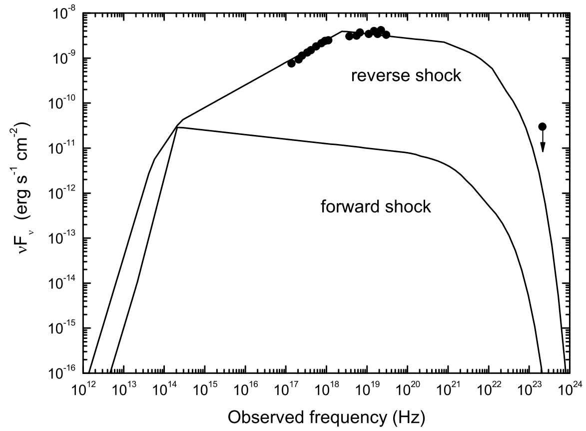

Figure 3. The spectral energy distribution of Swift J1644+57 at 31 hours after BAT trigger. The points show the observation data, which are taken from Burrows et al. (2011). The two lines represent the unabsorbed spectrum of the reverse and forward shocks, which are generated by the internal shock. The parameters of two shocks are given in the text.

In Figure 3, we fit the spectrum data from Burrows et al. (2011) detected at the same period. We adopt the parameters as follow: $L_4 = L_1 = L = 10^{48.5}$erg s^{-1}, $\gamma_4 = 1000$, $\gamma_1 = 10$, $\delta t = 100$ s, $\epsilon_e = 0.8$, and $\epsilon_B = 0.001$. Since shocks produced by collisions are highly nonlinearly processes, therefore the microscopic parameters, i.e. ϵ_e and ϵ_B, can be different for different collisions.

The X-ray flux from Swift J1644+57 is observed to

[1] We can see that these characteristic frequencies, i.e. ν_c and ν_m, are very sensitive to the Lorentz factor. However, Kobayashi et al. (1997) have shown that the radiation loss is less than 10% of total energy, therefore there is virtually no evolution of these spectral parameters during the collision.

track the X-ray hardness (Bloom et al. 2011; Levan et al. 2011). The X-ray flux and photon index exhibit a strong anti-correlation. This signature is a natural consequence of our model. In the earlier stage when the the internal shocks is dominated the X-ray flux is high but variable and harder. At later time when the external shock is dominated, the X-ray flux becomes lower but less fluctuating and softer.

The durations of flares are very complicated, similar as the X-ray flares in GRBs. For individual flare, the duration can be roughly estimated as Δ/c, where Δ is the width of shell (Maxham & Zhang 2009). If the ejecta are coming from the disk around the black hole, it should have the size of disk $r_d \sim 3r_s \sim 6GM/c^2 \sim 8\times10^{11}M_6$ cm, where M is the mass of black hole. From the minimum rise time, Bloom et al. (2011) and Burrows et al. (2011) have estimated $M_6 \sim 10$. So the duration of individual flare should be of order of $\Delta/c \sim r_d/c \sim 200$ s. However, flares can superimpose on each other if shells collide near the same time. For example, the duration of the flare detected at 111045 s after BAT trigger is about 300 s, which is consistent with the rise time scale. But the duration of the flare at about 1.115×10^5 s after BAT trigger with minimum rise time is longer than 1000 s. We believe that this flare is a superposition of several flares. It is interesting to note that the flares detected in GRBs indicate that the shell width Δ broadens with ejected time. A natural broadening mechanism is shell spreading. After a shell enters the spreading regime, the width of the shell is proportional to the radius, so that if the collision radius is larger the duration of X-ray flare can last longer. In this event, we can also see that the width of flares broadens with ejected time. This is similar to some central engine models of GRBs, for example, in the fragmented disk model proposed by Perna et al. (2006), the clumps at larger radius have lower densities and tend to be more spread out so that the accretion time scale is longer.

4 SUMMARY

In this letter, we propose the internal shock model to explain the X-ray flares of Swift J1644+57. In the internal shock model, collisions between a series of relativistic shells generate many pairs of forward and reverse shocks. The synchrotron emission produced by the forward and reverse shocks could dominate at two quite different energy bands if the Lorentz factors of these two types of shocks are significantly different from each other. We show that the spectral energy distribution of Swift J1644+57 could be fitted in internal shock model, in which the reverse shock is relativistic and the forward shock is Newtonian. A moderate extinction ($A_V = 3-5$) is required, this value is consistent with that used in Bloom et al. (2011) and Burrows et al. (2011). Burrows et al. (2011) showed that the high frequency spectrum is produced by the synchrotron and SSC mechanisms, similar to poynting flux-dominated blazar jet model. The radio fluxes come from a larger region of the other jet. This model requires continuous in situ re-acceleration of electrons to maintain a low energy cut-off in the electron distribution (Aliu et al. 2011). Bloom et al. (2011) presented two models for the spectrum: one is two-component blazar emission model, the other is forward shock emission from jet-ISM interaction plus EIC emission model. But on the high frequency side, the LAT and VERITAS upper limits require that the SSC component is suppressed by $\gamma-\gamma$ pair production. The soft photons from the disk outflow may provide sources for the $\gamma-\gamma$ production.

The rapid rise and decline of the light curve may indicate the internal shock origin of these flares. The external shock is very hard to account for the X-ray flares (Burrows et al. 2005; Fan & Wei 2005; Zhang et al. 2006). During the high state, the emission of internal shock will dominate at X-ray band and a broken power-law spectrum is shown. During the low state, there is no internal shock and the emission is from external shock. The spectrum at X-ray band will be shown as a single power-law if no energy injection happens. In both states, the radio emission is from the external shock.

ACKNOWLEDGMENTS

We thank the referee for his/her detailed and very constructive suggestions that have allowed us to improve our manuscript. We also thank Dr. Y. W. Yu and R. Li for useful discussion. K. S. Cheng is supported by the GRF Grants of the Government of the Hong Kong SAR under HKU 7011/10P. F. Y. Wang is supported by the National Natural Science Foundation of China (grant no. 11103007), Jiangsu Planned Projects for Postdoctoral Research Funds 1002006B and China Postdoctoral Science Foundation funded projects (20100481117 and 201104521).

REFERENCES

Aliu, A., et al. 2011, ApJ, 738, L30
Blandford, R. D., & McKee, C. F. 1976, Phys. Fluids, 19, 1130
Blandford, R. D., & Znajek, R. L. 1977, MNRAS, 179, 433
Bloom, J. S., et al. 2011, Science, 333, 203
Burrows, D. N., et al. 2005, Science, 309, 1833
Burrows, D. N., et al. 2011, Nature, 476, 421
Campana, S., et al. 2011, GCN 11851
Cannizzo, J. K., Troja, E., & Lodato, G. 2011, ApJ, 742, 32
Cheng, K. S. & Lu, Y. 2001, MNRAS, 320, 235
Cheng, K. S. & Wei, D. M. 1996, MNRAS, 283, L133
Cummings, J. R., et al. 2011, GCN 11823
Dai, Z. G., & Lu, T. 2002, ApJ, 565, L87
Fan, Y. Z., & Piran, T. 2008, Front. Phys. China, 3, 306
Fan, Y. Z., & Wei, D. M. 2005, MNRAS, 364, L42
Giannios D., & Metzger B. D., 2011, MNRAS, 416, 2102
Huang Y. F., Cheng, K. S. & Gao, T. T., 2006, ApJ, 637, 873
Kobayashi, S., Piran, T. & Sari, R. 1997, ApJ, 490, 92
Krolik, J. H., & Piran, T. 2011, arXiv: 1106.0923
Levan, A. J., et al. 2011, Science, 333, 199
Maxham, A. & Zhang, B. 2009, ApJ, 707, 1623
Metzger, B. D., Giannios, D. & Mimica, P. arXiv: 1110.1111
Paczyński, B. & Xu, G. H. 1994, ApJ, 427, 708
Panaitescu, A., & Kumar, P. 2000, ApJ, 543, 66
Perna, R., Armitage, P. J., & Zhang, B. 2006, ApJ, 636, L29
Proga, D., & Zhang, B. 2006, MNRAS, 370, L61

Rees, M. J. & Mészáros, P. 1994, ApJ, 430, L93
Sakamoto, T., et al. 2011, GCN, 11842
Sari, R. & Piran, T. 1995, ApJ, 455, L143
Sari, R., Piran, T., & Narayan, R. 1998, ApJ, 497, L17
Shao, L., Zhang, F. W., Fan, Y. Z. & Wei, D. M. 2011, ApJ, 734, L33
Socrates, A. 2011, arXiv: 1105.2557
Strubbe, L. E. & Quataert, E. 2009, MNRAS, 400, 2070
Wijers, R. A. M. J. & Galama, T. J. 1999, ApJ, 523, 177
Yu, Y. W., & Dai, Z. G. 2009, ApJ, 692, 133
Yu, Y. W., Wang. X. Y., & Dai, Z. G. 2009, ApJ, 692, 1662
Zauderer, B. A., et al. 2011, Nature, 476, 425
Zhang, B., et al., 2006, ApJ, 642, 354
Zhang, B. & Mészáros, P. 2002, ApJ, 566, 712